Unmanned Systems, Vol. 14, No. 2 (2026) 369–378

DOI: 10.1142/S2301385026500056

UNMANNED SYSTEMS
https://www.worldscientific.com/worldscinet/us

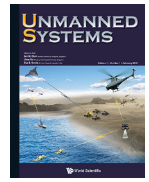

Plane-Aware Heightmap for Adaptable Footstep Planning in Discontinuous Coplanar Terrain

Chao Li [*], Yongliang Shi [†], Chencheng Dong [*], Qingqing Li [*,‡], Xuechao Chen [*], Zhangguo Yu [*], Zhihong Jiang [*]

[*]*School of Mechatronical Engineering, Beijing Institute of Technology, Beijing 100081, P. R. China*

[†]*Qiyuan Lab, Beijing 100095, P. R. China*

Planar information is crucial for determining the support plane of a candidate footstep, enabling reliable traversability checks during footstep planning. Due to the imprudent determination of the support plane caused by insufficient planar information, current heightmap-based algorithms struggle to plan footsteps in discontinuous coplanar terrain. In this paper, we propose a plane-aware heightmap that integrates the results of planar region detection, allowing each cell to direct retrieval of its corresponding plane parameters. Building on this, the support plane of a candidate footstep is determined by evaluating the consistency between the support planes of the four corner subregions of the foot. Specifically, the support plane considered for each corner subregion is the one with the highest elevation within that region, provided it is sufficiently large to support the corresponding area. We evaluate the enhancement of footstep planning achieved by the proposed heightmap and support-plane determination methods, which enable planning across diverse discontinuous coplanar terrain in both simulated and real-world settings.

Keywords: Biped robot; plane-aware heightmap; footstep planning; support plane determination.

1. Introduction

In recent years, unmanned systems [1, 2], especially biomimetic robots [3], have experienced notable advancements with the help of key components [4]. Bipedal robots have garnered widespread attention recently due to their high traversability across various terrains. As a common terrain, discontinuous coplanar terrain presents a significant challenge, making it crucial for robots to navigate such terrain autonomously.

Planar regions are typically considered feasible in structured environments because they offer even and stable foot support. Some researchers [5–8] represent the environment using planar regions, allowing for the assessment of a candidate footstep's traversability by checking if the contour of a planar region encloses the landing area [5, 6, 9, 10], with this plane serving as the corresponding support plane. Compared to planar regions, heightmaps are becoming increasingly popular due to their simplicity, versatility, and efficient computation [11–16]. However, the lack of detailed planar parameters in current heightmaps often leads to determining the support plane by evaluating the coplanarity of all points within a subregion of the landing area [17, 18]. This region-based approach is imprudent, as supporting the foot does not require an entire planar region to support the landing point; instead, it only relies on key dispersed load-bearing patches to provide adequate support. This limitation reduces the adaptability of footstep planning and limits the robot's ability to traverse discontinuous coplanar terrain effectively.

This work introduces a plane-aware heightmap as a terrain representation for footstep planning. The heightmap incorporates the results of planar grid region extraction,

Received 3 October 2024; Accepted 6 January 2025; Published 18 March 2025. This paper was recommended for publication in its revised form by editorial board member, Shenghai Yuan.
Email Address: ‡*7520230130@bit.edu.cn*
‡Corresponding author.

where each grid cell contains the plane parameters of its corresponding planar region. To reliably determine the support plane for a candidate footstep, we evaluate the consistency between the support planes of the four corner subregions of the foot to determine the overall support plane for the foot. The support plane for each subregion is identified as the plane with the highest elevation and a sufficiently large support area. If the support planes of the four corner subregions are consistent, this plane is adopted as the support plane for the candidate footstep. Both simulated and real-world experiments demonstrate that our method enhances adaptability to diverse discontinuous coplanar terrains.

The major contributions of this paper are highlighted as follows:

(1) We introduce a novel plane-aware heightmap that integrates the results of planar grid region extraction, where each grid cell contains its corresponding planar parameters. This heightmap directly provides planar parameters from the environment by cell index, which are used to determine the support plane of the four corner subregions.
(2) We propose a reliable support-plane determination method based on a plane-aware heightmap, reducing the risk of misjudging the traversability of candidate footsteps in discontinuous coplanar terrains. The support plane for a candidate footstep is determined by assessing the consistency between the support planes of the four corner subregions, which are defined as the planes with the highest elevation and a sufficiently large support area within their corresponding regions.
(3) We validated the proposed mapping and support-plane determination methods through simulations and real-world experiments, demonstrating that they improve the robot's ability to navigate diverse discontinuous coplanar terrains.

The remainder of this paper is organized as follows. The following section discusses the related works about the perception method for bipedal walking. Section 3 introduces the proposed method, and Sec. 4 experimentally evaluates the proposed method and compares it with current approaches. Finally, Sec. 5 concludes this paper.

2. Related Work

Some works represent the environment as a set of planar regions. Kumagai *et al.* [19] used a HeightField and an OctoMap to represent the environment, with the former used for planar region detection and the latter for frequent collision checks. The footstep planner replans footsteps based on location during continuous walking. Fallon *et al.* [7] employed the Kintinuous [20] algorithm to fuse stereo images continuously and applied a feature clustering-based method to generate the terrain for footstep planning [9]. The Florida Institute for Human and Machine Cognition (IHMC) [6] developed an algorithm to extract planar regions from collected depth images by combining region growing and patch graph techniques. Accelerated by an NVIDIA GTX 970 GPU, this algorithm requires only 5–6 ms, enabling biped robots to stably and continuously walk over irregular terrain [21], along with other related works [10, 22, 23]. Bertrand *et al.* [5] presented the environment as an OctoMap [24] collected by a rotating UTM-30LX-EW device and used a nearest-neighbor search approach to detect planar regions. Lee *et al.* [8, 25] developed a camera-laser fusion system to obtain a stable and dense point cloud for segmenting specific objects in outdoor environments. Their perceptual algorithm fitted square planar regions by combining super-pixel segmentation with random sampling.

Some works [11, 26, 27] described the environment as a heightmap. Yamamoto *et al.* [17] expressed the environment as a stochastic Elevation-and-Normal Grid (ENG) map whose cell contains the elevation, normal direction, and the standard deviation of measurements, allowing the robot to traverse through uneven terrain stably after the traversability check. When checking the traversability of a candidate footstep, it is necessary first to calculate the support plane coefficients using the cells of a subregion in the landing area. This approach is unreasonable. Ueda *et al.* [28] used a fast plane detection algorithm [29] to extract planar information from the input depth image and expressed it as 2D planar occupancy grids in the 3D space. Gutmann *et al.* [30] used heightmap to present stairs and obstacles to navigate for biped robots. Helei *et al.* [31] used depth images and robot state to train a heightmap predictor, which builds a heightmap of the local terrain, enabling biped robots to navigate challenging terrains effectively. Fankhauser *et al.* [13, 32] incorporated the drift and uncertainties of state estimation to create a probabilistic terrain estimate, which is then used to construct a robot-centric elevation map. Miki *et al.* [33] efficiently created an elevation map with additional features using a GPU for navigation. Gian *et al.* [34] integrated multi-modal information, including semantic and appearance data, into an elevation map to create a universal map. Based on the heightmap mentioned above, Takahiro *et al.* [35] integrated exteroceptive and proprioceptive perception for locomotion. They used reinforcement learning (RL) to generate a legged locomotion controller with high robustness and speed, enabling the robot to walk through a variety of challenging natural and urban environments. Tranzatto *et al.* [14] used this elevation map to accomplish collaborative exploration tasks. Mastalli *et al.* [15] and Jenelten *et al.* [36] represented terrain as an elevation map and used this map for motion optimization during locomotion. Wermelinger *et al.* [37] used an elevation map to compute typical terrain characteristics such as slope, roughness, and steps to build a feasible map. They combined this map with a sampling-based planner to navigate complex terrains.

An excellent case [38] for biped robots' navigation used scan-line grouping to extract arbitrary planes in the robot's view, which can dispose of the noise dynamics of stereo vision well. In this system, the 3D environment map for the biped robot locomotion planning is constructed utilizing the occupancy grid and the floor heightmaps from the extracted planes. This method combines the robot's multi-modal motion with the map representation, which satisfies the robot's navigation requirements well.

3. Method

3.1. *Construct plane-aware heightmap*

3.1.1. *Construct heightmap*

Preprocess. Before constructing a heightmap, preprocessing of the point cloud is typically necessary. This preprocessing includes voxel filtering, removal of flying points, and passthrough filtering.

Voxel filtering aims to reduce noise and redundancy by representing each voxel with the centroid (average position) of all points within it. The purpose of removing flying points is to eliminate points located in the projection shadows of objects that do not correspond to any physically present objects in the scene. Flying point is typically identified and filtered out based on the angle between the normal and the direction of each point. Passthrough filtering removes interfering data from the point cloud, such as the robot's knees, while retaining other environmental data.

Construct Heightmap. After preprocessing, the resulting point cloud is transformed into the robot's coordinate system. Based on the transformed point cloud, a heightmap in the robot's coordinate system is constructed (as shown in Fig. 1(b)). The heightmap uses a two-dimensional grid to represent the height of a three-dimensional terrain, with each grid cell storing a height value.

3.1.2. *Integrate plane extraction results into the heightmap*

Extract Planar Grid Region. Based on the constructed heightmap, we extract planar regions that satisfy the robot's locomotion constraints. First, we convert the heightmap into an organized point cloud and then use PEAC [39] for planar region extraction, the extraction results as shown in Fig. 1(c). This algorithm initially divides the point cloud into patches and constructs a graph based on the patches and their neighbors. Finally, the nodes that belong to the same plane are merged using an agglomerative hierarchical clustering algorithm.

Merge Planar Regions that Belong to the Same Plane. Although planar regions have been extracted from the heightmap, different planar regions that belong to the same plane still need to be merged into a single region. This step facilitates determining the support plane of a candidate footstep, as the entire foot's support plane is defined by whether the support areas of the forefoot and hindfoot are consistent. The merging result is shown in Fig. 1(d).

Label Each Cell with a Plane-index. Based on the merging results, each cell is labeled with a plane index using a one-to-one mapping between the organized point cloud and the cell index in the heightmap. This allows for the direct retrieval of the plane parameters associated with each cell, resulting in a plane-aware heightmap, as shown in Fig. 1(e).

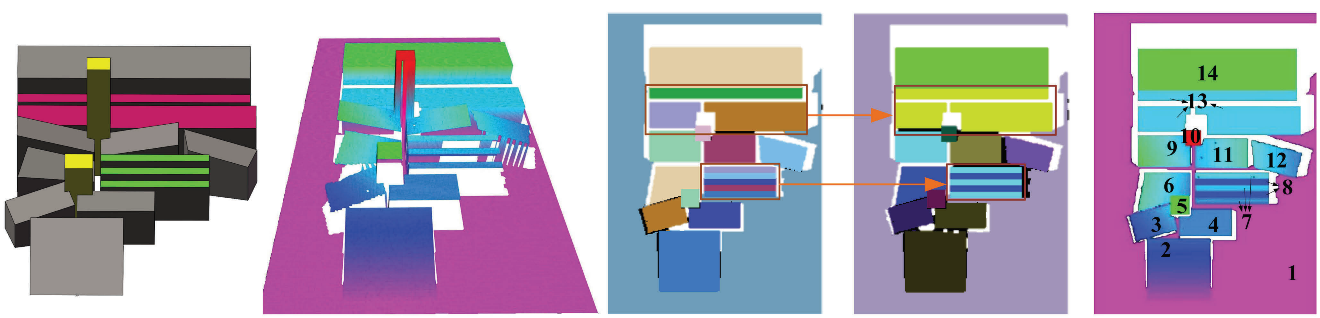

(a) (b) (c) (d) (e)

Fig. 1. The construction process of the plane-aware heightmap. (a) Although the green areas and red areas belong to different planar regions due to being disconnected, each set is part of its respective plane. (b) The constructed heightmap. (c) The results of the planar region extraction. (d) The planar regions after merging regions that belong to the same plane. (e) Plane-aware heightmap. Each cell in the heightmap is labeled with a plane index, allowing the corresponding planar parameters to be retrieved directly from the index.

3.2. *Footstep planning and support plane determination*

3.2.1. *Footstep planning*

Our footstep planning algorithm is a weighted A* algorithm [18, 26]. It consists of two main steps: node expansion and node scoring. Node expansion involves evaluating a fixed set of candidate nodes relative to the current node. During expansion, we check the traversability of each candidate node. Node scoring comprises two components: greedy and heuristic. The greedy component (g) accounts for the distance traveled from the start to the current node, while the heuristic component considers both the distance to the goal (h_1) and angular differences relative to the goal (h_2). The details are shown in Fig. 2.

$$f = \alpha g + \beta h_1 + \gamma h_2, \tag{1}$$

where f represents the score of a node, which corresponds to the node's cost. g denotes the node's greedy component, while h_1 and h_2 represent its heuristic components. The coefficients α, β, γ are the respective weights assigned to these terms.

$$g = \|n - n_{\text{parent}}\| + g_{\text{parent}}, \tag{2}$$

where $\|n - n_{\text{parent}}\|$ represents the horizontal distance between the node and its parent node. g_{parent} denotes the greedy component of the parent node. If the node has no parent, g is set to 0.

$$h_1 = \|n_g - n\|, \tag{3}$$

where $\|n_g - n\|$ represents the horizontal distance between the node and the goal.

$$h_2 = |\text{ori}_{n_g} - \text{ori}_n|, \tag{4}$$

where $|\text{ori}_{n_g} - \text{ori}_n|$ represents the difference in orientation angles on the horizontal plane between the node and the goal.

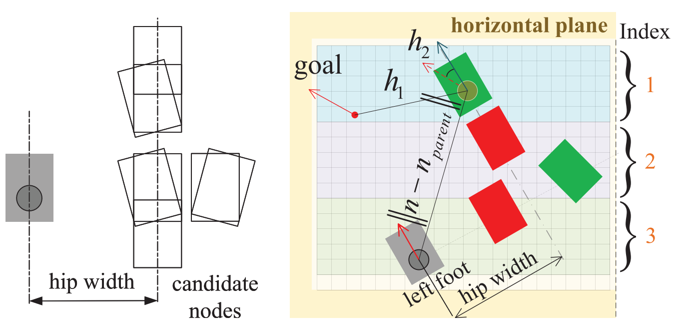

(a) (b)

Fig. 2. Introduction of footstep planning. (a) Represents a fixed set of candidate nodes during the expansion of nodes. (b) Each cell in the heightmap contains a plane index label. Initially, some untraversable nodes are removed from the original candidate set. For example, red nodes are removed because the support planes of the four corner subregions are inconsistent, or some grid cells in the corresponding landing areas penetrate the support plane. Green nodes, on the other hand, are considered traversable. These traversable nodes are then scored, with the greedy component representing the distance traveled from the start to the current node ($\|n - n_{\text{parent}}\| + g_{\text{parent}}$) and the heuristic component considering both the distance to the goal (h_1) and orientation differences relative to the goal (h_2).

3.2.2. *Support plane determination*

Previous heightmap-based methods for determining the support plane relied on evaluating the coplanarity of cells within a subregion around the landing point, an approach deemed imprudent [17, 18]. The foot's support does not depend on the entire planar region but instead relies on dispersed load-bearing patches that adequately support the landing point. To address this limitation, this paper uses four corner sub-regions of the foot to determine the support plane based on the proposed plane-aware heightmap. The specific approach is as follows: First, the plane indices of all cells within the landing areas of the four corner sub-regions are counted. The plane with the highest elevation and a count exceeding a specified threshold is selected as the support plane for the respective area. If the identified support planes for the four corners are consistent, this plane is adopted as the overall support plane for the candidate footstep. The details are shown in Fig. 3. Traversability is checked by ensuring no grid cells penetrate the foot's support plane.

For a candidate footstep spanning discontinuous but coplanar steps, our proposed method effectively identifies their support planes, enabling reliable traversability assessments.

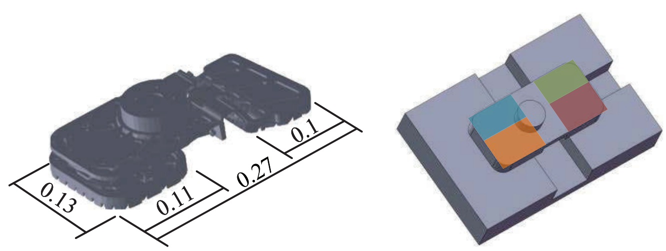

(a) (b)

Fig. 3. Determining the support plane process. (a) The parameters of the foot. (b) The four corner sub-regions of the foot (four colored patches) are assessed to determine the overall support plane. The foot's support plane is determined when the support planes of these four sub-regions are consistent. Each sub-region's support plane is identified as the one with the highest elevation within that area, as long as the plane is sufficiently large to support the corresponding sub-region.

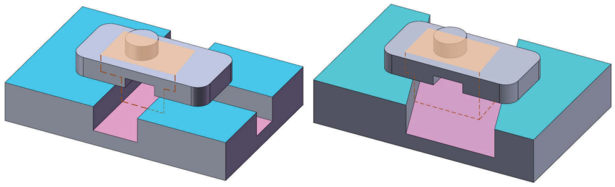

Fig. 4. Two candidate footsteps span discontinuous but coplanar steps. Using the proposed method, the support planes for the four corner subregions are correctly identified as the blue plane, resulting in the overall support plane for the foot being the blue plane, which aligns with the actual support surface at landing. In contrast, existing methods [17, 18] first evaluate whether the area surrounding the landing point (illustrated as the brownish-yellow region) is coplanar and then assign the coplanar plane as the support plane. However, this approach fails to correctly determine the support planes for these footsteps, misclassifying them as untraversable — significant misjudgment.

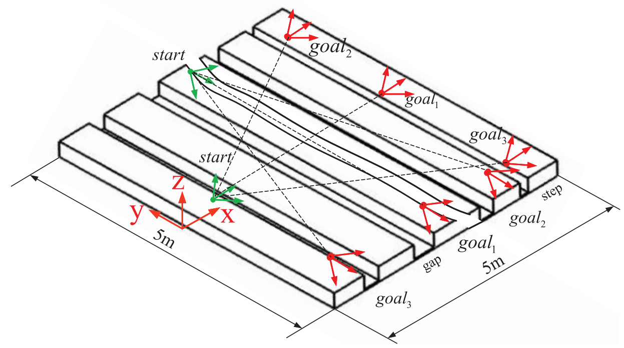

Fig. 5. Discontinuous coplanar steps, along with the planned start and goals. The step width ranges from 5 to 27 cm, and the gap width ranges from 5 to 14 cm, determined by the fabrication and installation of the steps as well as the robot's locomotion ability. The start (0.3, 0) and the goals (4.5, 0), (4.5, −2), and (4.5, 2) form one set of points, with each point associated with three possible directions. This set provides 27 start and goal pairs for planning. Another set consists of the start (2.5, 2) and the goals (2.5, −2), (4.5, −2), and (0.5, −2), also resulting in 27 planning start and goal pairs.

This capability enhances the robot's adaptability to such challenging terrain. In contrast, existing methods rely on evaluating the coplanarity of the regions surrounding the landing point of a candidate footstep. As a result, they often fail to correctly determine the support plane, misclassifying inherently traversable footsteps as untraversable. This misjudgment reduces the number of viable footsteps available during node expansion, requiring more footsteps to reach the goal on such terrain. Details are illustrated in Fig. 4.

4. Experiments

4.1. *Simulated environments*

This paper focuses on enhancing the robot's adaptability to discontinuous coplanar terrains, a scenario commonly encountered on wooden boardwalks in parks. To evaluate the adaptability of the proposed algorithm to such terrain, step and gap widths were randomly generated within a 5 m × 5 m terrain map, sequentially filling it with steps and gaps, as shown in Fig. 5. The green point and red points represent the candidate start and goal positions for footstep planning. Suitable start and goal points are selected within a circle centered on these points, with the radius equal to the diagonal length of the robot's foot.

The planning results, as summarized in Table 1, demonstrate that the proposed algorithm exhibits strong adaptability to discontinuous coplanar terrain. This adaptability stems from its capability to accurately determine the support plane for candidate footsteps spanning multiple coplanar steps, facilitating step planning to reach the goal. In contrast, existing algorithms [17, 18] typically require candidate footsteps to be fully supported by a single step, limiting their adaptability in these scenarios. One exception (highlighted in italics) occurred because, in this case, the robot's left and right feet remained on their respective steps during the planning process and did not traverse across the discontinuous coplanar terrain. However, such scenarios are beyond the primary focus of this study, which targets navigation across discontinuous coplanar steps.

The above scenarios involve regular step-gap configurations. To further evaluate the algorithm, several random scenarios are constructed by transforming the regular steps into wavy steps. Additionally, a random phase shift was applied between adjacent wavy steps to ensure the randomness of the discontinuous coplanar terrain, as shown in Fig. 6. The experimental results are presented in Table 2, which shows that the proposed algorithm demonstrates stronger adaptability to this type of random terrain compared to existing algorithms [17, 18]. Moreover, in most cases, the efficiency of planning is significantly improved. The results also indicate that the proposed method plans fewer footsteps to reach the goal. This advantage arises from the algorithms' ability to accurately identify the support planes of candidate footsteps that span multiple steps, significantly reducing the likelihood of misclassifying traversable candidate footsteps as non-traversable. As a result, each expansion is performed from nodes closer to the goal, thereby reaching the goal with fewer footsteps.

4.2. *Real-world environment*

4.2.1. *Platform*

The BHR-8P is a position-controlled biped robot of our team, which weighs 72 kg and stands 1.6 m tall. It has 26

Table 1. Planning results in discontinuous coplanar steps.

Terrain information:	16 10 25 12 8 9 17 14 18 11 22 12 22 13 18 12 14 9 27 7 25 6 17 13 24 13 27 5 27 12 18 12 5			
(0.300 0.000 0.000) (4.500 0.000 0.000)	(0.300 0.000 0.000) (4.500 0.000 0.785)	(0.300 0.000 0.000) (4.400 2.000 −0.785)	(0.300 0.000 0.000) (4.400 −2.000 0.000)	(0.300 0.000 0.000) (4.400 −2.000 0.785)
error start	error start	error start	error start	error start
16559.632 8276.081 16659 0.497 59	11797.111 5616.118 11274 0.498 76	12148.599 6210.637 12444 0.499 103	9985.358 5255.330 10593 0.496 76	17323.034 8512.306 17409 0.489 99
(2.500 2.000 −1.571) (2.500 −2.000 −1.571)	(2.500 2.000 −1.571) (2.500 −2.000 −0.785)	(2.500 2.000 −1.571) (4.500 −2.000 −2.356)	(2.500 2.000 −1.571) (0.500 −2.000 −1.571)	(2.500 2.000 −1.571) (0.500 −2.000 −0.785)
2737.781 642.497 5057 0.127 74	error goal	error goal	error goal	error goal
4776.085 2296.164 4678 0.491 77	7817.573 3981.047 7928 0.502 69	37391.237 22128.893 44474 0.498 109	4439.716 2287.071 4676 0.489 75	9052.832 4172.351 8489 0.492 123

Notes. The first row of the table represents terrain information, described as a sequence of numbers alternating between the width of a step and the width of a gap, with all measurements in centimeters.

The second row indicates the planning start and goal, where each parameter is specified as follows: x-coordinate (meters), y-coordinate (meters), and yaw angle (radians). The third and fourth rows present the planning results of existing methods [17, 18] and the proposed method for the specified start and goal points. "error start/goal" indicates that no suitable start or goal point could be found nearby, while "error planning" signifies that the planning process either timed out (exceeding 3 min) or failed to generate a plan. The successful planning result (e.g. 16559.632 8276.081 16659 0.497 59) is interpreted as follows: The first value represents the planning duration (milliseconds). The second value indicates the total duration for support plane determination (milliseconds). The third value corresponds to the average duration for support plane determination (milliseconds). The fourth value indicates the total number of support plane determinations. The subsequent rows follow the same structure as described above.

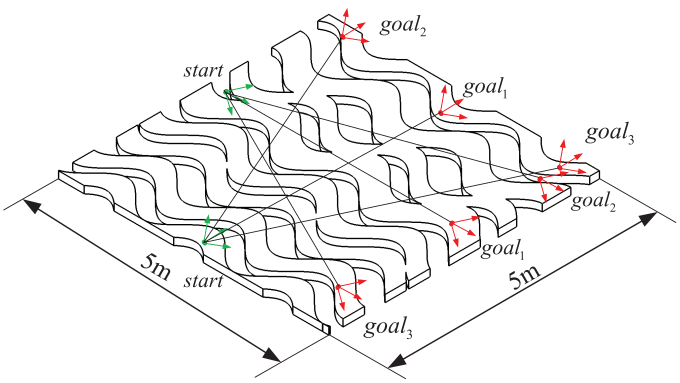

Fig. 6. Discontinuous coplanar wavy steps, along with the planned start and goals. The regular steps in Fig. 5 were transformed into wave steps, with a random phase shift introduced between adjacent steps.

degrees of freedom (DoF) for the whole body, which are 6 DoF per leg and 7 DoF per arm (Fig. 8). The control computer is a NUC8 with a 2.3 GHz Intel i5-8259U processor, and the control rate is 250 Hz. Due to limitations in the robot's joint motion range and the capabilities of its stability control algorithm, the robot's step length is restricted to a maximum of 0.33 m. This constraint directly impacts the parameter settings in our footstep planning algorithm, specifically limiting the maximum x-direction distance between a parent node and its child node to 0.33 m during node expansion.

The proposed perception method is implemented on a mini-personal computer using an AMD Core R7-6800H of 3.2 GHz and 16 GB RAM. No parallelism was employed in its implementation, whether OpenMP, GPU, or multi-threading. The camera installed on BHR-8P is an Intel RealSense L515 (Fig. 8), which generates 640 × 480 depth images with high accuracy at 30 Hz and ensures the accuracy of the perceptual information. The camera (with a FOV of 75° × 55°) is installed at an angle of 45° with the vertical direction, and the installation height is 1.25 m.

4.2.2. *Experiments*

We conducted tests in two typical scenarios to verify the effectiveness of the proposed method combined with our stability controller [40–43].

As highlighted in Refs. 5 and 11, conducting experiments in larger environments can enhance the credibility and impact of our results. This typically involves using rotating or swing LiDAR to capture environmental data. However, the precision of the data from these sensors is insufficient to meet the demands of our control algorithm. In this work, we employ a ToF depth camera, which captures high-precision point clouds. However, its detection range is limited,

Table 2. Planning results in discontinuous coplanar wavy steps.

Terrain information:	6 5 6 5 6 32 15 14 47 10 9 1 17 9 40 17 12 33 9 10 35 10 13 26 18 13 26 14 5 28 8 10 22 9 9 1 23 8 36 16 13 28 12 8 39 16 9 49 17 6 39 8 13 34 10 9 48 26 8 11 24 10 45 5 11 3			
(0.200 0.000 −0.785) (4.700 −2.000 0.000)	(0.200 0.000 0.785) (4.700 2.000 −0.785)	(2.500 2.300 −1.571) (2.500 −2.200 −1.571)	(2.500 2.300 −1.571) (2.500 −2.200 −0.785)	(2.500 2.300 −0.785) (2.500 −2.200 −1.571)
67978.737 17466.422 136620 0.128 140	116429.031 22916.456 175506 0.131 141	33208.992 8614.376 66306 0.130 145	47756.636 14237.231 109659 0.130 130	60186.615 18701.636 145986 0.128 151
27592.517 18218.085 36738 0.496 101	25311.592 12973.283 26052 0.498 131	10317.183 6795.113 13701 0.496 96	13760.154 7160.152 14352 0.499 90	16878.638 8524.447 17010 0.501 64
(2.500 2.300 −1.571) (2.500 −2.200 −1.571)	(2.500 2.300 −1.571) (2.500 −2.200 −0.785)	(2.500 2.300 −2.356) (2.500 −2.200 −1.571)	(2.500 2.300 −2.356) (2.500 −2.200 −0.785)	(2.500 2.300 −2.356) (0.500 −2.200 −1.571)
20591.945 5281.434 40941 0.129 126	error planning	*17173.422 4740.927 36756 0.129 109*	error planning	60105.004 13491.878 105651 0.128 144
26313.491 20717.863 41727 0.497 116	73983.943 53072.850 105987 0.501 150	*43541.441 33469.974 67359 0.497 91*	66261.561 49188.534 98832 0.498 90	30128.233 21691.273 43920 0.494 112

Notes. The first row of the table represents terrain information, described as a sequence of numbers alternating between the width of a step, the width of a gap and a random phase shift, with all measurements in centimeters.

reliably providing terrain data within approximately 2 m in front of the robot. Within this smaller environment, we arranged discontinuous, coplanar steps to validate the effectiveness of the proposed method.

After collecting the current terrain data using the L515, the point cloud is transformed into the robot's coordinate system, which aligns with the map coordinate system (as shown in Fig. 8(a)), and a heightmap is constructed. Since the robot's knees obstruct the area in front of its feet, pass-through filtering is applied during heightmap construction to remove data affected by knee interference. However, this filtering results in missing data for the region in front of the robot's feet. To address this, we compensate for the missing data by filling the area with a point cloud of zero height.

The dimensions of each element in the real-world scenario are shown in Fig. 7. The wooden step is too narrow to provide independent support for a foot. The distance between adjacent steps is 0.2 m, requiring a stride of over 0.36 m to cross this narrow step, which is unfriendly for this robot. Existing methods fail to correctly identify the support planes of candidate footsteps when a candidate footstep spans multiple steps within the robot's locomotion capability. As a result, these methods cannot plan a feasible sequence of footsteps to reach the goal. However, the proposed method accurately determines the support plane of a candidate footstep spanning multiple steps, enabling reliable traversability assessment and ensuring that feasible footsteps can be planned to reach the goal—a capability

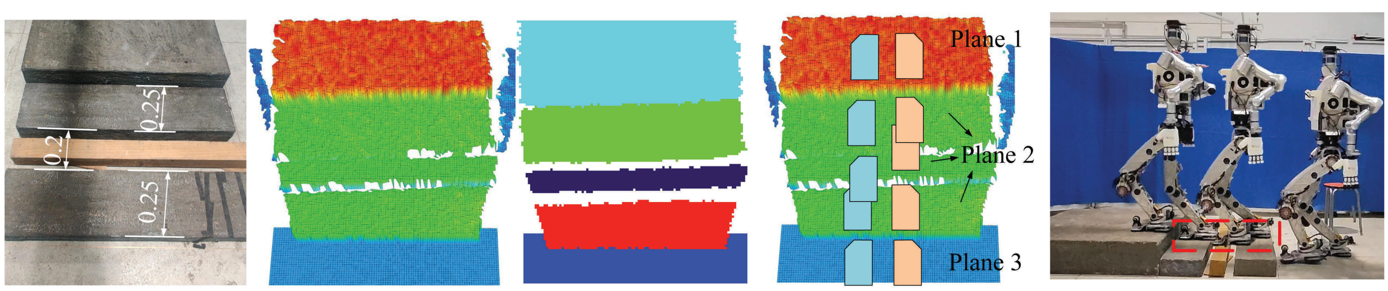

(a) (b) (c) (d) (e)

Fig. 7. The robot traverses a discontinuous coplanar terrain scenario containing a narrow step. (a) Real-world scenario. (b) The corresponding heightmap. (c) The planar region extraction results. Planar regions belonging to the same plane are merged, and a plane-aware heightmap is constructed based on the merged regions. (d) Utilizing this heightmap and the proposed support plane determination method, we can reliably identify the support plane for a candidate footstep spanning multiple steps. This approach improves the accuracy of traversability assessments and facilitates footstep planning toward the goal, enhancing the robot's adaptability to discontinuous coplanar terrain containing narrow steps. (e) A real-world experiment.

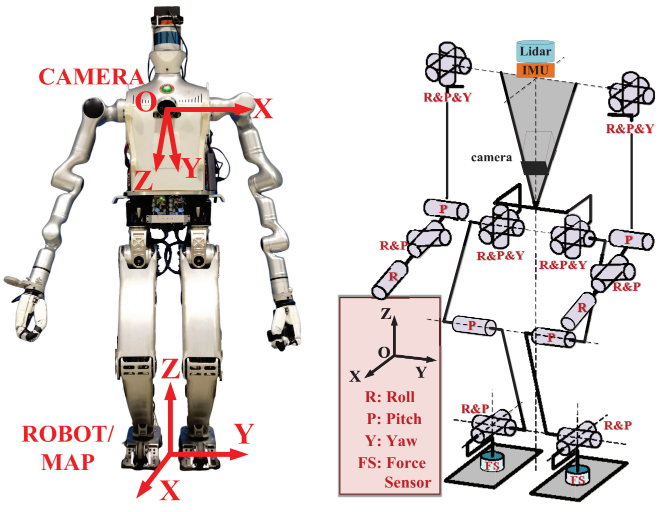

(a) (b)

Fig. 8. Depiction of BHR-8P. (a) BHR-8P. (b) Abstracted model of BHR-8P.

that existing methods [17, 18] lack. This significantly enhances the robot's adaptability to discontinuous coplanar terrain, a common scenario in park boardwalks.

5. Conclusion

This work proposes a plane-aware heightmap for terrain representation, which integrates plane region extraction results, allowing direct access to the corresponding planar parameters of each cell by its index. Building on this heightmap, we introduce a novel method for determining the support plane of a candidate footstep during the footstep planning process. This method determines the overall support plane of the foot by evaluating whether the support planes of its four corner subregions are consistent. The support plane for each corner subregion is selected as the one with the highest elevation within that region, provided it is sufficiently large to support the corresponding area. This approach effectively determines the support plane of a candidate footstep that lands on multiple steps, increasing the reliability of traversability checks and enhancing the robot's adaptability to discontinuous coplanar terrain. We validated the proposed method through both simulations and real-world experiments. The results demonstrate that the proposed method improves adaptability in scenarios with discontinuous coplanar terrain, including narrow steps.

Acknowledgments

This work was supported by the Postdoctoral Fellowship Program of CPSF under Grant Number GZC20233399 and the Fundamental Research Funds for the Central Universities under Grant Number 2024CX06079.

ORCID

Chao Li https://orcid.org/0000-0003-4758-0498
Yongliang Shi https://orcid.org/0000-0003-3086-729X
Chencheng Dong https://orcid.org/0000-0002-2444-3637
Qingqing Li https://orcid.org/0000-0002-9888-4160
Xuechao Chen https://orcid.org/0000-0003-1136-3053
Zhangguo Yu https://orcid.org/0000-0003-0041-8100
Zhihong Jiang https://orcid.org/0000-0001-8133-6312

References

[1] P. Wu and J. Chen, Efficient box approximation for data-driven probabilistic geofencing, *Unmanned Syst.* **1** (2023) 1–12.
[2] P. Wu, X. Yang, P. Wei and J. Chen, Safety assured online guidance with airborne separation for urban air mobility operations in uncertain environments, *IEEE Trans. Intell. Transp. Syst.* **23**(10) (2022) 19413–19427.
[3] C. Li, J. Cao, W. Ouyang and Q. Ren, Motion control of bionic robots via biomimetic learning, *Unmanned Syst.* **6**(03) (2018) 165–174.
[4] P. Xiang, L. Yan, Y. Guo, X. He, C. Gerada and I.-M. Chen, A concentrated-flux-type pm machine with irregular magnets and iron poles, *IEEE/ASME Trans. Mechatronics* **29** (2023) 691–702.
[5] S. Bertrand, I. Lee, B. Mishra, D. Calvert, J. Pratt and R. Griffin, Detecting usable planar regions for legged robot locomotion, in *IEEE/RSJ Int. Conf. Intelligent Robots and Systems (IROS)* (IEEE, 2020), pp. 4736–4742.
[6] B. Mishra, D. Calvert, S. Bertrand, S. McCrory, R. Griffin and H. E. Sevil, Gpu-accelerated rapid planar region extraction for dynamic behaviors on legged robots, in *IEEE/RSJ Int. Conf. Intelligent Robots and Systems (IROS)* (IEEE, 2021), pp. 8493–8499.
[7] M. F. Fallon, P. Marion, R. Deits, T. Whelan, M. Antone, J. McDonald and R. Tedrake, Continuous humanoid locomotion over uneven terrain using stereo fusion, in *IEEE-RAS 15th Int. Conf. Humanoid Robots (Humanoids)* (IEEE, 2015), pp. 881–888.
[8] I. Shim, S. Shin, Y. Bok, K. Joo, D.-G. Choi, J.-Y. Lee, J. Park, J.-H. Oh and I. S. Kweon, Vision system and depth processing for drc-hubo+, in *IEEE Int. Conf. Robotics and Automation (ICRA)* (IEEE, 2016), pp. 2456–2463.
[9] R. Deits and R. Tedrake, Footstep planning on uneven terrain with mixed-integer convex optimization, in *IEEE-RAS Int. Conf. Humanoid Robots* (IEEE, 2014), pp. 279–286.
[10] R. J. Griffin, G. Wiedebach, S. McCrory, S. Bertrand, I. Lee and J. Pratt, Footstep planning for autonomous walking over rough terrain, in *IEEE-RAS 19th Int. Conf. Humanoid Robots (Humanoids)* (IEEE, 2019), pp. 9–16.

[11] K. Nishiwaki, J. Chestnutt and S. Kagami, Autonomous navigation of a humanoid robot over unknown rough terrain using a laser range sensor, *Int. J. Robot. Res.* **31**(11) (2012) 1251–1262.

[12] P. Fankhauser and M. Hutter, A universal grid map library: Implementation and use case for rough terrain navigation, in *Robot Operating System (ROS) The Complete Reference* (World Scientific, 2016), pp. 99–120.

[13] P. Fankhauser, M. Bloesch and M. Hutter, Probabilistic terrain mapping for mobile robots with uncertain localization, *IEEE Robot. Autom. Lett.* **3**(4) (2018) 3019–3026.

[14] M. Tranzatto *et al.*, Cerberus: Autonomous legged and aerial robotic exploration in the tunnel and urban circuits of the darpa subterranean challenge, preprint (2022), arXiv:2201.07067.

[15] C. Mastalli, I. Havoutis, M. Focchi, D. G. Caldwell and C. Semini, Motion planning for quadrupedal locomotion: Coupled planning, terrain mapping, and whole-body control, *IEEE Trans. Robot.* **36**(6) (2020) 1635–1648.

[16] H. Duan, B. Pandit, M. S. Gadde, B. J. van Marum, J. Dao, C. Kim and A. Fern, Learning vision-based bipedal locomotion for challenging terrain, preprint (2023), arXiv:2309.14594.

[17] T. Yamamoto and T. Sugihara, Responsive navigation of a biped robot that takes into account terrain, foot-reachability and capturability, *Adv. Robot.* **35**(8) (2021) 516–530.

[18] J. Chestnutt, J. Kuffner, K. Nishiwaki and S. Kagami, Planning biped navigation strategies in complex environments, in *IEEE Int. Conf. Humanoid Robotics* (IEEE, 2003).

[19] I. Kumagai, M. Morisawa, S. Nakaoka, T. Sakaguchi, H. Kaminaga, K. Kaneko and F. Kanehiro, Perception based locomotion system for a humanoid robot with adaptive footstep compensation under task constraints, in *IEEE/RSJ Int. Conf. Intelligent Robots and Systems (IROS)* (IEEE, 2018), pp. 713–719.

[20] T. Whelan, M. Kaess, H. Johannsson, M. Fallon, J. J. Leonard and J. McDonald, Real-time large-scale dense rgb-d slam with volumetric fusion, *Int. J. Robot. Res.* **34**(4–5) (2015) 598–626.

[21] D. Calvert, B. Mishra, S. McCrory, S. Bertrand, R. Griffin and J. Pratt, A fast, autonomous, bipedal walking behavior over rapid regions, preprint (2022), arXiv:2207.08312.

[22] S. McCrory, B. Mishra, J. An, R. Griffin, J. Pratt and H. E. Sevil, Humanoid path planning over rough terrain using traversability assessment, preprint (2022), arXiv:2203.00602.

[23] B. Mishra, D. Calvert, B. Ortolano, M. Asselmeier, L. Fina, S. McCrory, H. E. Sevil and R. Griffin, Perception engine using a multi-sensor head to enable high-level humanoid robot behaviors, in *Int. Conf. Robotics and Automation (ICRA)* (IEEE, 2022), pp. 9251–9257.

[24] A. Hornung, K. M. Wurm, M. Bennewitz, C. Stachniss and W. Burgard, Octomap: An efficient probabilistic 3d mapping framework based on octrees, *Auton. Robots* **34**(3) (2013) 189–206.

[25] I. Lee, J. Oh, I. Kim and J.-H. Oh, Camera-laser fusion sensor system and environmental recognition for humanoids in disaster scenarios, *J. Mech. Sci. Technol.* **31**(6) (2017) 2997–3003.

[26] D. Maier, C. Lutz and M. Bennewitz, Integrated perception, mapping, and footstep planning for humanoid navigation among 3d obstacles, in *IEEE/RSJ Int. Conf. Intelligent Robots and Systems* (IEEE, 2013), pp. 2658–2664.

[27] A. Stumpf, S. Kohlbrecher, D. C. Conner and O. von Stryk, Open source integrated 3d footstep planning framework for humanoid robots, in *IEEE-RAS 16th Int. Conf. Humanoid Robots (Humanoids)* (IEEE, 2016), pp. 938–945.

[28] R. Ueda, S. Nozawa, K. Okada and M. Inaba, Biped humanoid navigation system supervised through interruptible user-interface with asynchronous vision and foot sensor monitoring, in *IEEE-RAS Int. Conf. Humanoid Robots* (IEEE, 2014), pp. 273–278.

[29] A. J. Trevor, S. Gedikli, R. B. Rusu and H. I. Christensen, Efficient organized point cloud segmentation with connected components, *Semantic Perception Mapping and Exploration (SPME)* **10** (6) (2013) 251–257.

[30] J.-S. Gutmann, M. Fukuchi and M. Fujita, A floor and obstacle height map for 3d navigation of a humanoid robot, in *Proc. IEEE Int. Conf. Robotics and Automation* (IEEE, 2005), pp. 1066–1071.

[31] H. Duan, B. Pandit, M. S. Gadde, B. Van Marum, J. Dao, C. Kim and A. Fern, Learning vision-based bipedal locomotion for challenging terrain, in *IEEE Int. Conf. Robotics and Automation (ICRA)* (IEEE, 2024), pp. 56–62.

[32] P. Fankhauser, M. Bloesch, C. Gehring, M. Hutter and R. Siegwart, Robot-centric elevation mapping with uncertainty estimates, in *Mobile Service Robotics* (World Scientific, 2014), pp. 433–440.

[33] T. Miki, L. Wellhausen, R. Grandia, F. Jenelten, T. Homberger and M. Hutter, Elevation mapping for locomotion and navigation using gpu, in *IEEE/RSJ Int. Conf. Intelligent Robots and Systems (IROS)* (IEEE, 2022), pp. 2273–2280.

[34] G. Erni, J. Frey, T. Miki, M. Mattamala and M. Hutter, Mem: Multimodal elevation mapping for robotics and learning, in *IEEE/RSJ Int. Conf. Intelligent Robots and Systems (IROS)* (IEEE, 2023), pp. 11011–11018.

[35] T. Miki, J. Lee, J. Hwangbo, L. Wellhausen, V. Koltun and M. Hutter, Learning robust perceptive locomotion for quadrupedal robots in the wild, *Sci. Robot.* **7**(62) (2022) eabk2822.

[36] F. Jenelten, R. Grandia, F. Farshidian and M. Hutter, Tamols: Terrain-aware motion optimization for legged systems, *IEEE Trans. Robot.* **38**(6) (2022) 3395–3413.

[37] M. Wermelinger, P. Fankhauser, R. Diethelm, P. Krüsi, R. Siegwart and M. Hutter, Navigation planning for legged robots in challenging terrain, in *IEEE/RSJ Int. Conf. Intelligent Robots and Systems (IROS)* (IEEE, 2016), pp. 1184–1189.

[38] J.-S. Gutmann, M. Fukuchi and M. Fujita, 3d perception and environment map generation for humanoid robot navigation, *Int. J. Robot. Res.* **27**(10) (2008) 1117–1134.

[39] C. Feng, Y. Taguchi and V. R. Kamat, Fast plane extraction in organized point clouds using agglomerative hierarchical clustering, in *IEEE Int. Conf. Robotics and Automation (ICRA)* (IEEE, 2014), pp. 6218–6225.

[40] Q. Li, F. Meng, Z. Yu, X. Chen and Q. Huang, Dynamic torso compliance control for standing and walking balance of position-controlled humanoid robots, *IEEE/ASME Trans. Mechatronics* **26**(2) (2021) 679–688.

[41] C. Dong, X. Chen, Z. Yu, H. Chen, Q. Li and Q. Huang, Reactive bipedal balance: Coordinating compliance and stepping through virtual model imitation for enhanced stability, *Expert Syst. Appl.* (2024) 124334.

[42] C. Dong, Z. Yu, X. Chen, H. Chen, Y. Huang and Q. Huang, Adaptability control towards complex ground based on fuzzy logic for humanoid robots, *IEEE Trans. Fuzzy Syst.* **30**(6) (2022) 1574–1584.

[43] L. Han, X. Chen, Z. Yu, J. Zhang, Z. Gao and Q. Huang, Enhancing speed recovery rapidity in bipedal walking with limited foot area using dcm predictions, *Expert Syst. Appl.* **250** (2024) 123858.

Chao Li received his B.S. degree from the Hubei University of Automotive Technology (HUAT) in 2014 and the M.S. degree from the Beijing Institute of Technology (BIT) in 2020. He is currently working toward his Ph.D. degree in mechanical engineering with Intelligent Robotics Institute, School of Mechatronic Engineering, BIT. His research interests environment perception and navigation for biped robots.

Yongliang Shi obtained his Ph.D. in mechatronics engineering from the Beijing Institute of Technology, Beijing, China, in 2021. His research focuses on Neural Radiance Fields (NeRF), simultaneous localization and mapping (SLAM), and multi-sensor fusion-based localization for robots.

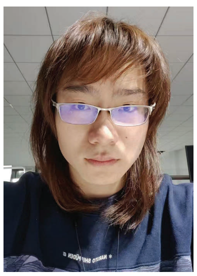

Chencheng Dong received his B.S. degree in mechatronics engineering from Beijing Institute of Technology (BIT), Beijing, China, in 2019. He is currently a Ph.D. candidate with the Intelligent Robotics Institute, School of Mechatronic Engineering, BIT, Beijing, China. His research interests include biped walking and running stability control, and compliance control.

Qingqing Li received his B.S. degree in mechatronics engineering from the Henan University of Science and Technology, Luoyang, China, in 2015, and the Ph. D. degree in mechatronics engineering from the Beijing Institute of Technology (BIT), Beijing, China, in 2023. He is currently a Postdoctoral Research Fellow with the School of Mechatronic Engineering, BIT. His research interests include bipedal motion planning and stability control of biped robots.

Xuechao Chen received his B.S. and Ph.D. degrees in mechatronics engineering from the BIT in 2007 and 2013, respectively. He was a Visiting Student with the Robotics Institute, Carnegie Mellon University, Pittsburgh, PA, USA, in 2012. Since July 2013, he has been a Professor with the School of Mechatronics Engineering, BIT. Dr. Chen received a First Class Prize of the Ministry of Education Award for Technology Invention.

Zhangguo Yu received his B.S. and M.S. degrees in control engineering from the Southwest University of Science and Technology (SWUST), China, in 1997 and 2005, respectively, and the Ph.D. degree in mechatronics engineering from the BIT in 2009. He was as an Associate Professor with SWUST between 2001 and 2009. He was a Visiting Scholar with the University of Electro-Communications, Tokyo, Japan, in 2011. He is currently a Professor with the BIT.

Zhihong Jiang was born in Jiangsu, China. He received his B.S. and M.S. degrees in material processing and manufacturing engineering from the Jilin University of Technology, Changchun, China, in 1998 and 2001, respectively, and the Ph.D. degree in electrical engineering and automation from Tsinghua University, Beijing, China, in 2005. He is currently a Professor with the School of Mechatronical Engineering, Beijing Institute of Technology, Beijing, China. His research interests include space intelligent robotics, industry robot systems, artificial intelligence and robot vision, and human–machine interaction.